Supporting Information

# Contents

1 Supporting Figures
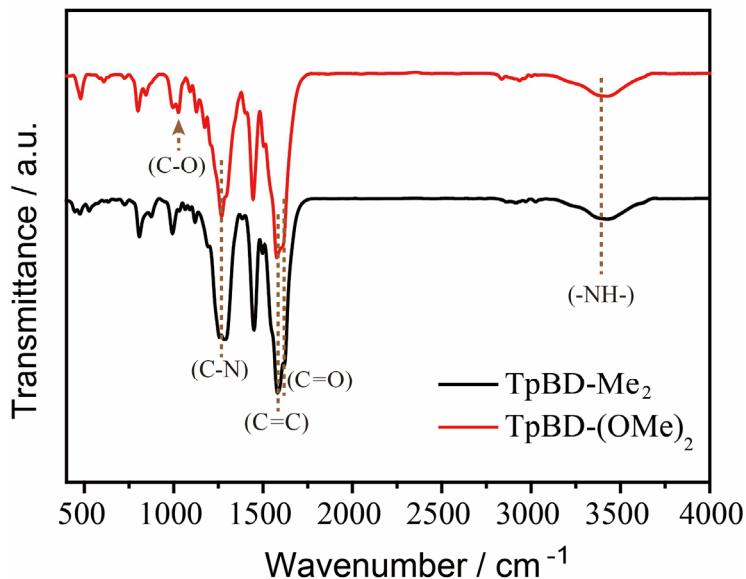
**Figure S1** The FT-IR spectra of TpBD-Me$_2$ and TpBD-(OMe)$_2$ and the characteristic peaks are marked on the photos.
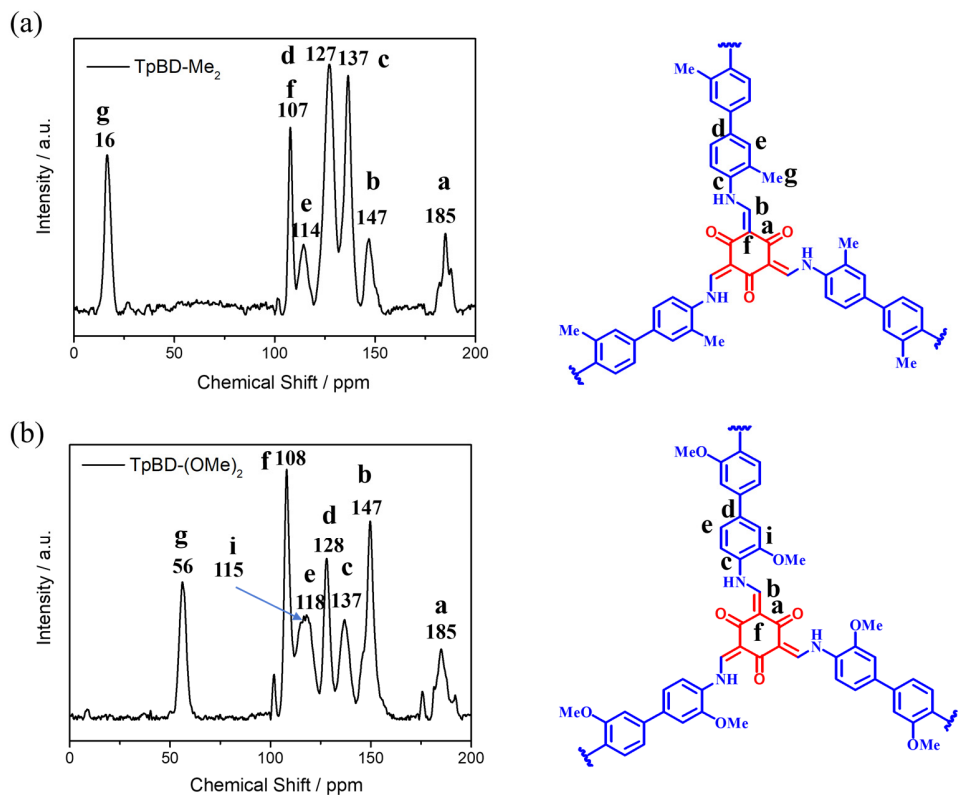
Figure S2 Solid-state ^{13}C CP-MAS NMR spectra of TpBD-Me$_2$ (a) and TpBD-(OMe)$_2$ (b), in which the chemical shifts of carbon in different environments are marked in the photos.
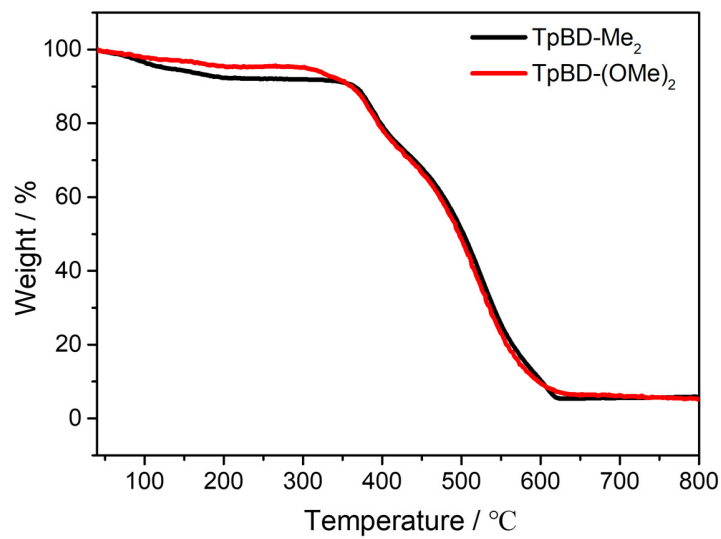
Figure S3 Thermogravimetric analysis (TGA) profiles of TpBD-Me$_2$ and TpBD-(OMe)$_2$ obtained in the temperature range from 25°C to 800°C.
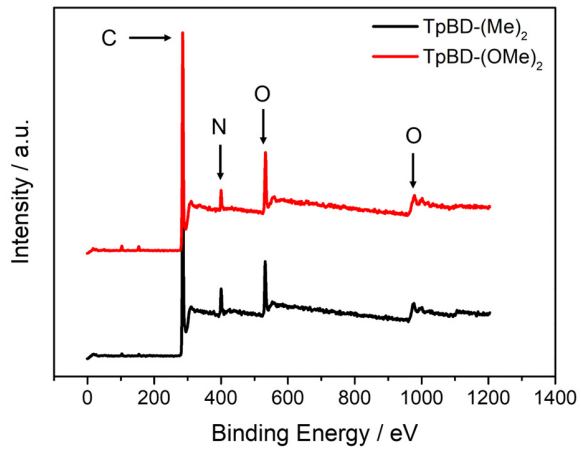
Figure S4 XPS spectra of TpBD-Me$_2$ (black), TpBD-(OMe)$_2$ (red), in which the peaks of C, O and N are marked with arrows.
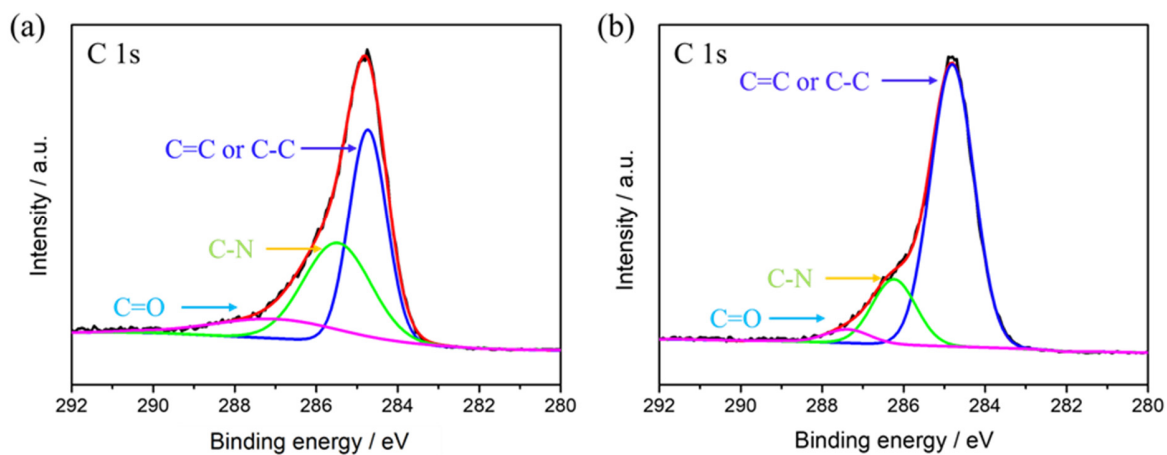
Figure S5 High-resolution XPS spectra of C1s for TpBD-Me$_2$ (a) and TpBD-(OMe)$_2$ (b), which can be divided into three different carbon environments.
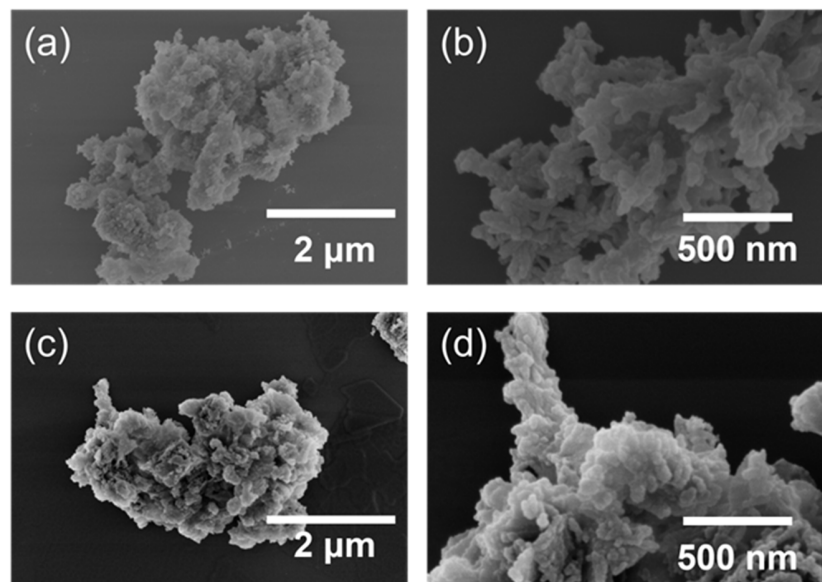
Figure S6 Low (a,c) and high (b,d) magnification SEM images of TpBD-Me$_2$ (a,b) and TpBD-(OMe)$_2$ (c,d) powders.
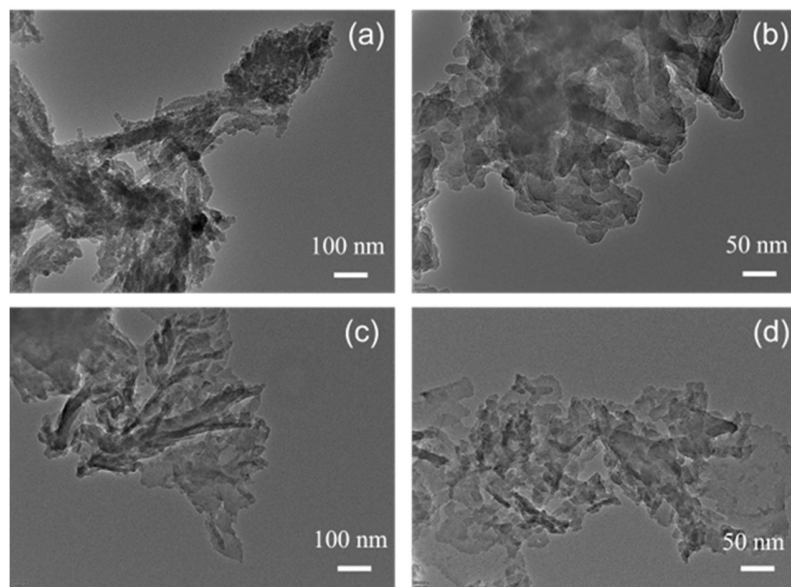
Figure S7 The TEM images of TpBD-Me$_2$ (a,b) and TpBD-(OMe)$_2$ (c,d) powders with different magnifications.
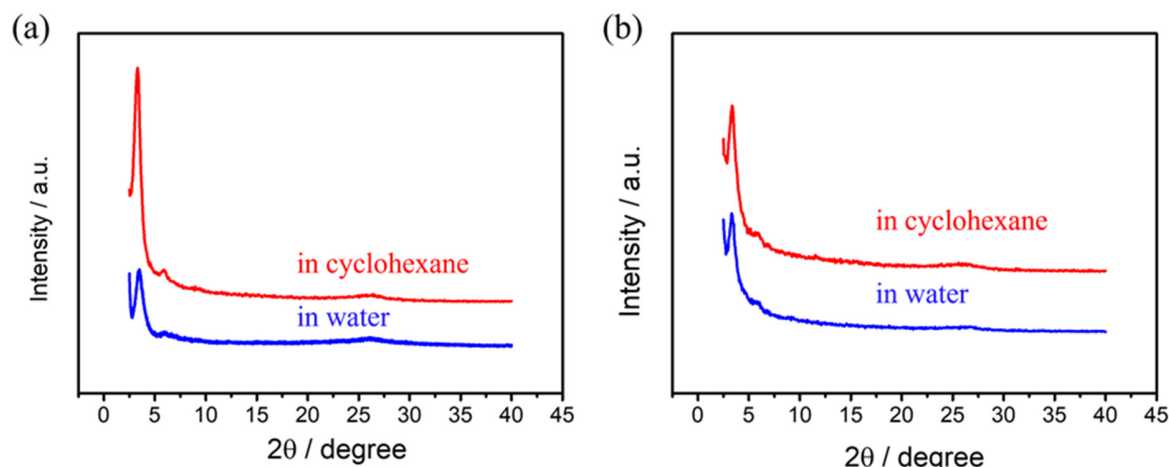
Figure S8 PXRD patterns of TpBD-Me$_2$ (a) and TpBD-(OMe)$_2$ (b) powders immersing in water and cyclohexane for two weeks without refreshing solvent. Prior to PXRD measurements, the samples were separated via filtration and followed by drying under vacuum at 100℃ for 48 hours.
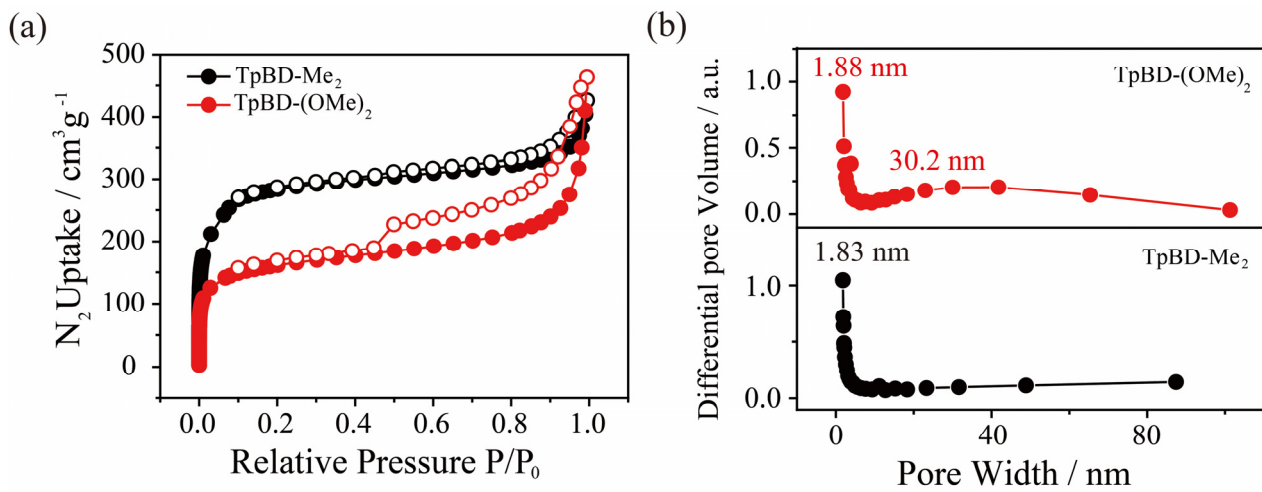
Figure S9 (a) Nitrogen adsorption-desorption isotherms curves of TpBD-Me$_2$ and TpBD-(OMe)$_2$ (filled circles: adsorption, open circles: desorption) (b) The pore size distribution of TpBD-Me$_2$ and TpBD-(OMe)$_2$.
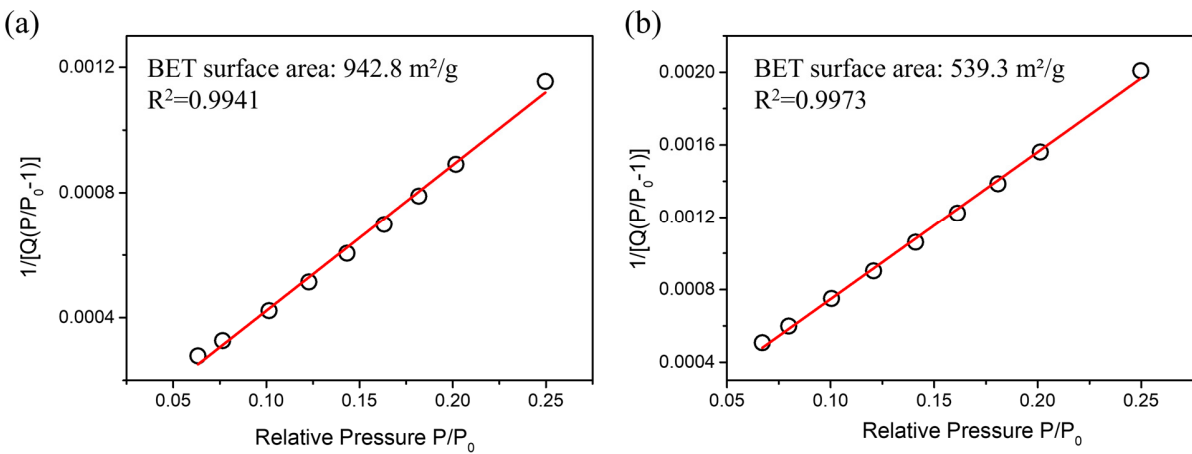
Figure S10 Plots of BET surface area of TpBD-Me$_2$ (a) and TpBD-(OMe)$_2$ (b) obtained by in the range of relative pressure 0-0.25 and the calculated value of the specific surface area and the values of R^2 for linear fitting are marked on the photos.
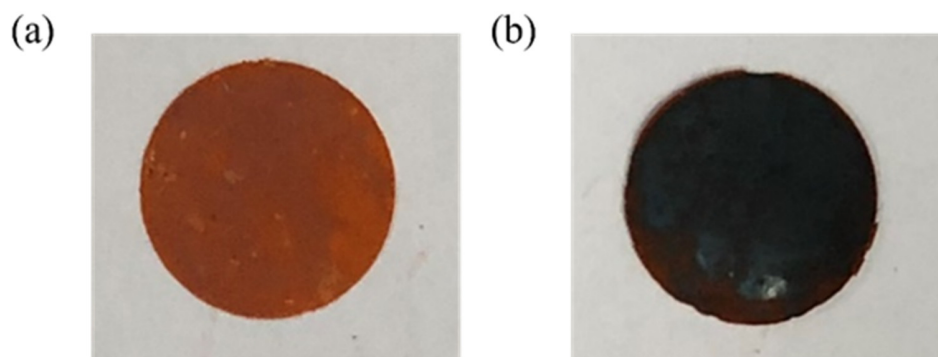
Figure S11 Photos of as-prepared disk-shaped sheet of TpBD-Me$_2$ (a) and TpBD-(OMe)$_2$ (b) which were obtained by pressing the powders with a tablet press at a pressure of 10 MPa for 1 minute.
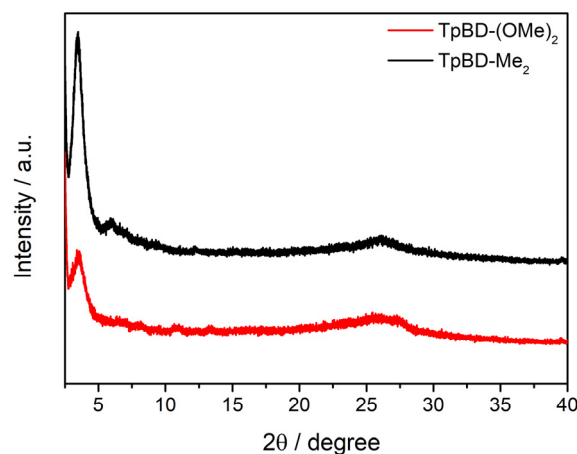
Figure S12 PXRD patterns of as-prepared TpBD-Me$_2$ and TpBD-(OMe)$_2$ sheets after being pressed at a pressure of 10 MPa.
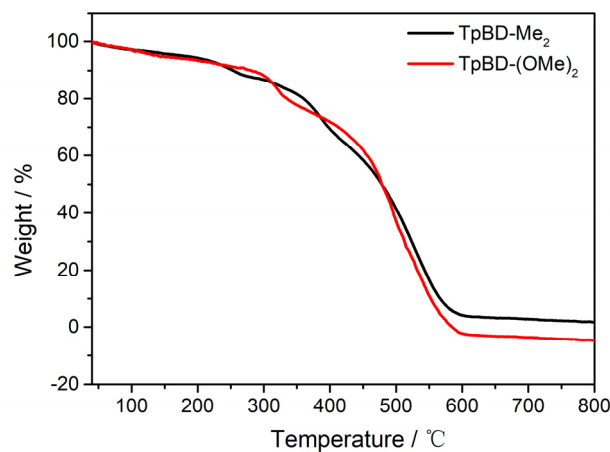
Figure S13 Thermogravimetric analysis (TGA) profiles of TpBD-Me$_2$ and TpBD-(OMe)$_2$ sheets after being pressed at a pressure of 10 MPa.
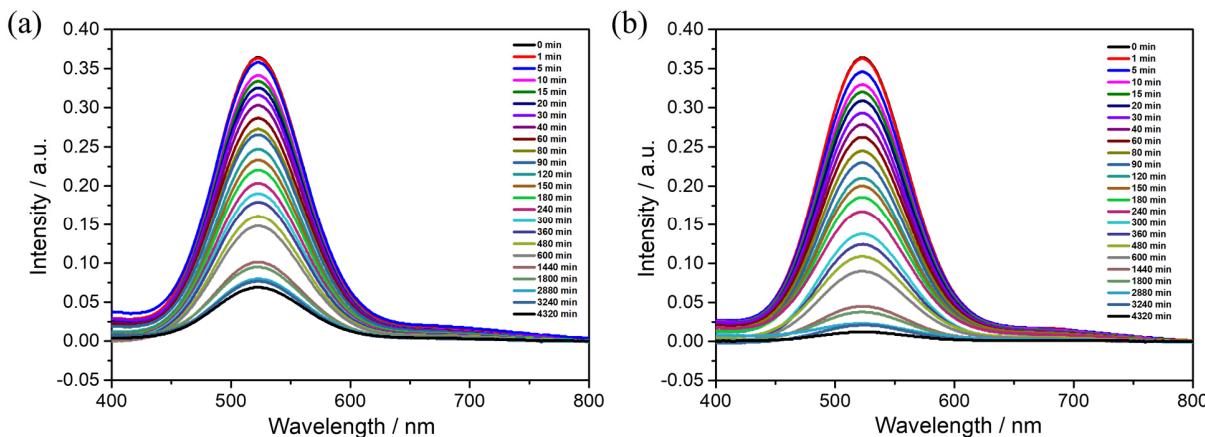
Figure S14 Temporal absorption spectral evolution of 10 mL of cyclohexane solution of I$_2$ at the initial concentration of 100.25 mg·L^{-1} recorded after 10 mg of TpBD-Me$_2$ (a) TpBD-(OMe)$_2$ (b) are placed inside.
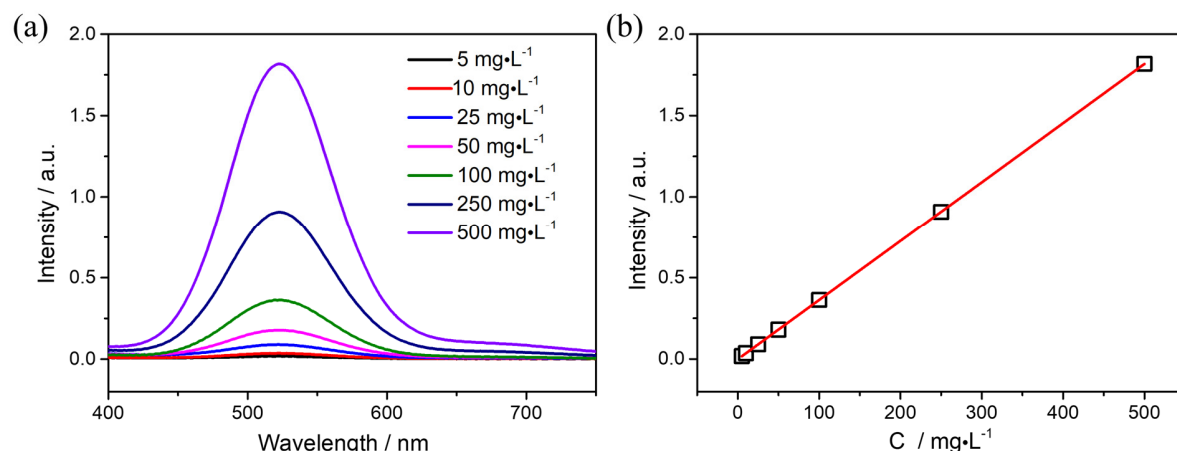
Figure S15 (a) UV-Vis spectra of cyclohexane solutions of I$_2$ at different concentration ranging from 5, to 10, 25, 50, 100, 250 and 500 mg·L^{-1}.(b) Plot of the absorption intensity of I$_2$ at about 520 nm versus the I$_2$ concentration (C, mg·L^{-1}) in cyclohexane, which can be fitted according to a linear function of Intensity = 0.00364 - 0.0009065C with r^2 of 0.9999.
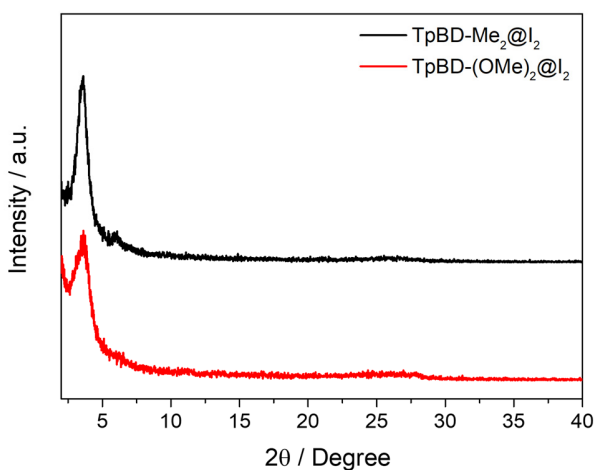
Figure S16 PXRD patterns of TpBD-Me$_2$@I$_2$ (black) and TpBD-(OMe)$_2$@I$_2$ (red) after I$_2$ adsorption in cyclohexane at initial concentration of 100 mg·L^{-1}.
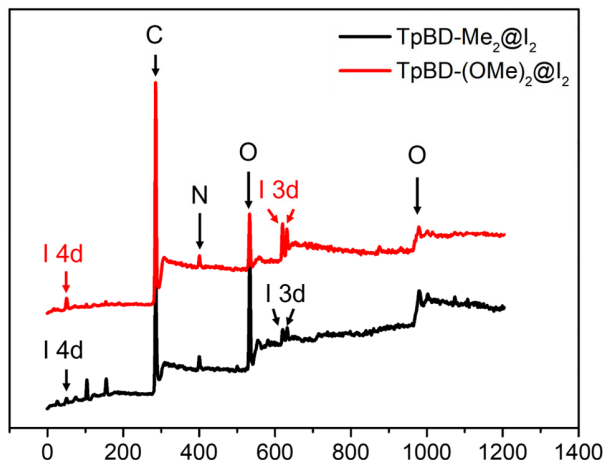
Figure S17 XPS spectra of TpBD-Me$_2$@I$_2$ and TpBD-(OMe)$_2$@I$_2$ obtained by 72 h adsorption of TpBD-Me$_2$ and TpBD-(OMe)$_2$ in the cyclohexane solutions of I$_2$ at 500 mg·L^{-1}.
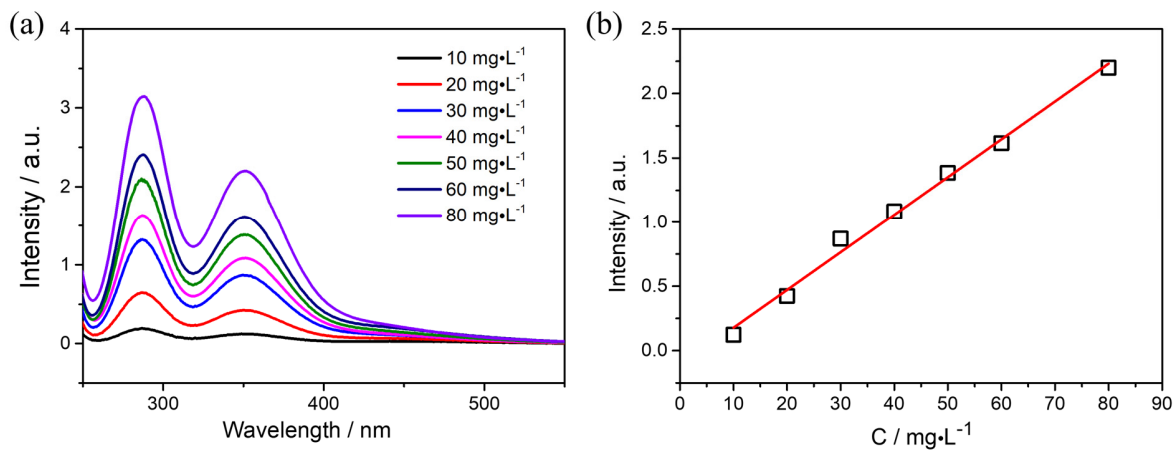
Figure S18 (a) UV-vis spectra of I_3^- aqueous solution (a mixture of KI and I_2 in the mole ration of 5:1) at concentration ranging from 10, to 20, 30, 40, 50, 60 and 80 mg·L^{-1} of I_2. (b) Plot of the absorbance intensity of I_3^- aqueous solution at 350 nm (I_{350}) versus I_2 concentration, which can be well fitted by a linear function, $I_{350} = 0.02935C_{I2} - 0.1156$ with $r^2=0.992$.
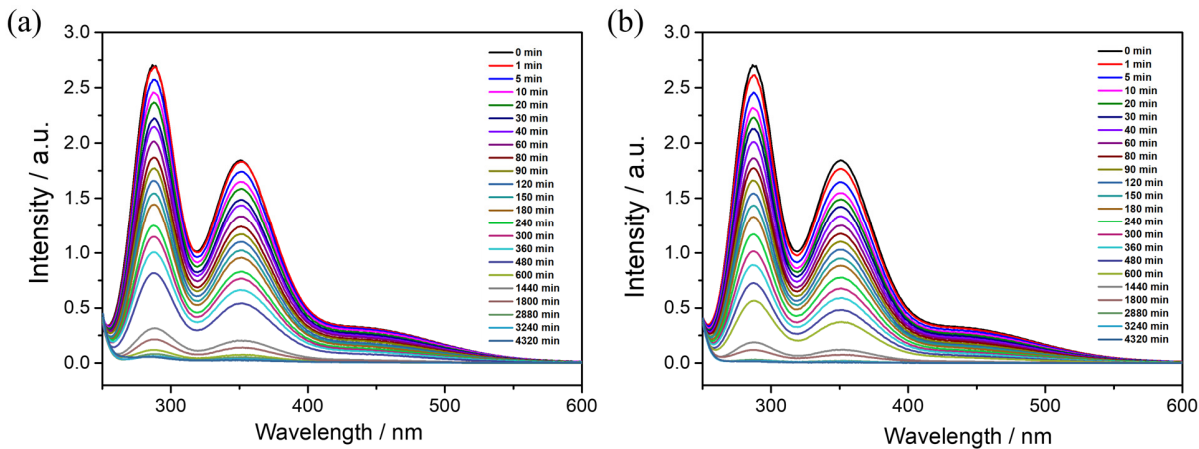
Figure S19 Temporal absorption spectral evolution of 10 mL aqueous solution of I_2/KI at the initial concentration of 66.67 mg·L^{-1} of I_2. recorded after 5 mg of TpBD-Me$_2$(a) TpBD-(OMe)$_2$(b) are placed inside.
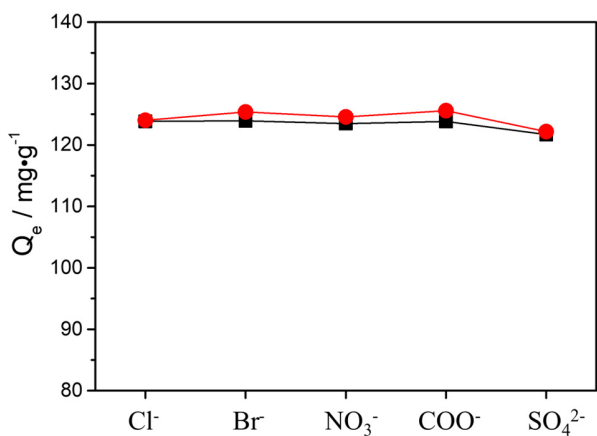
Figure S20 Plot of the values of Q_e of TpBD-Me2 (black square) and TpBD-(OMe)2 (red circle) in the presence of different kinds of competing anions, in which I2 adsorption is carried out at the initial concentration of 67 mg·L^{-1} of I2 in KI/I2 aqueous solution.
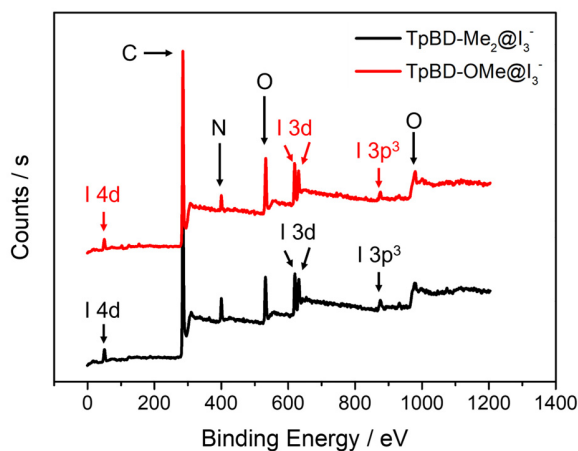
Figure S21 XPS spectra of TpBD-Me2@I3$^-$ (black) and TpBD-(OMe)2@ I3$^-$ obtained by 72 h adsorption of TpBD-Me2 and TpBD-(OMe)2 in the I3$^-$ aqueous solution (a mixture of KI and I2 in the mole ration of 5:1) at the presence of 200 mg·L^{-1} of I2.

2   Supporting Tables

Table S1 Summary of C, N, O atomic concentration of TpBD-Me$_2$ and TpBD-(OMe)$_2$ derived from the results of survey XPS spectra in Figure S4.

COFs	C	O	N
TpBD-Me$_2$	81.11%	10.49%	8.40%
TpBD-(OMe)$_2$	82.69%	11.87%	5.44%

Table S2 Summary of the BET fitting results of nitrogen adsorption isotherms of TpBD-Me$_2$ and TpBD-(OMe)$_2$.

COFs	Surface areas / m$^2 \cdot$g^{-1}	Pore volume / cm$^3 \cdot$g^{-1}	Pore diameter / nm
TpBD-Me$_2$	942.81	0.66	1.83
TpBD-(OMe)$_2$	539.30	0.72	1.88

Table S3 Summary of the values of q_t , q_t^{uc} and q_t^{Mol} of TpBD-Me$_2$ and TpBD-(OMe)$_2$ obtained during 72 h (4320 min) adsorption of I$_2$ in cyclohexane.

Time / min	TpBD-Me$_2$			TpBD-(OMe)$_2$		
	q_t/mg$\cdot$g^{-1}	q_t^{uc}/g$\cdot$moL^{-1}	q_t^{Mol}	q_t/mg$\cdot$g^{-1}	q_t^{uc}/g$\cdot$moL^{-1}	q_t^{Mol}
1	0.28	0.27	0.00105	0.28	0.29	0.00115
5	1.65	1.57	0.00617	4.95	5.17	0.0204
10	6.32	6.00	0.0236	9.34	9.76	0.0385
15	8.24	7.82	0.0308	12.09	12.64	0.0498
20	10.72	10.17	0.0401	15.11	15.79	0.0622
30	13.19	12.52	0.0493	19.51	20.39	0.0803
40	16.76	15.91	0.0627	23.35	24.40	0.0962
60	21.15	20.07	0.0791	28.02	29.29	0.115
80	25.00	23.73	0.0935	32.69	34.17	0.135
90	27.20	25.82	0.102	36.81	38.47	0.152
120	32.14	30.51	0.120	42.31	44.22	0.172
150	35.99	34.16	0.135	45.06	47.09	0.186
180	39.56	37.55	0.148	49.18	51.40	0.203
240	44.23	41.98	0.165	54.12	56.56	0.223
300	47.80	45.37	0.179	62.09	64.89	0.256
360	50.83	48.25	0.190	65.66	68.62	0.270

480	55.77	52.93	0.209	70.06	73.22	0.289
600	59.34	56.32	0.222	75.28	78.68	0.310
1440	72.25	68.58	0.270	87.65	91.61	0.361
1800	73.90	70.14	0.276	89.56	93.60	0.369
2880	78.02	74.05	0.292	93.68	97.91	0.386
3240	78.85	74.84	0.295	94.23	98.48	0.388
4320	80.77	76.66	0.302	95.61	99.93	0.394

Table S4 Summary of the experimental values of q_e (exp. q_e) of TpBD-Me$_2$ and TpBD-(OMe)$_2$ obtained by 72 h adsorption of I$_2$ in cyclohexane at initial concentration of 100.25 mg·L^{-1} and the calculated value of q_e (cal. q_e) from fitting of their adsorption kinetics profiles according to pseudo-first-order or pseudo-second-order models. The kinetic parameters obtained by fitting according to pseudo-first-order or pseudo-second-order models are also listed in the Table S4.

COFs	exp. q_e /mg·g^{-1}	Pseudo-first-order model			Pseudo-second-order model		
		cal. q_e /mg·g^{-1}	k_1/min^{-1}	R^2	cal. q_e /mg·g^{-1}	k_2/g·mg^{-1}·min^{-1}	R^2
TpBD-Me$_2$	80.77	74.34	0.004	0.969	81.95	6.316E-5	0.995
TpBD-(OMe)$_2$	95.61	88.70	0.005	0.965	97.10	6.441E-5	0.993

Table S5 Summary of the experimental values of q_e^{uc} (exp. q_e^{uc}) of TpBD-Me$_2$ and TpBD-(OMe)$_2$ obtained by 72 h adsorption of I$_2$ in cyclohexane at initial concentration of 100.25 mg·L^{-1} and the calculated value of q_e^{uc} (cal. q_e^{uc}) from fitting of their adsorption kinetics profiles according to pseudo-first-order or pseudo-second-order models. The kinetic parameters obtained by fitting according to pseudo-first-order or pseudo-second-order models are also listed in the Table S5.

COFs	exp. q_e^{uc} /g·mol^{-1}	Pseudo-first-order model			Pseudo-second-order model		
		cal. q_e^{uc} /g·mol^{-1}	k_1/min^{-1}	R^2	cal. q_e^{uc} /g·mol^{-1}	k_2/mol·g^{-1}·min^{-1}	R^2
TpBD-Me$_2$	76.66	70.56	0.004	0.969	77.78	6.655E-5	0.995
TpBD-(OMe)$_2$	99.93	92.71	0.005	0.965	101.48	6.163 E-5	0.993

Table S6 Summary of the values of q_t^{N+CO} of TpBD-Me$_2$ and q_t^{N+O}, q_t^{EO} of TpBD-(OMe)$_2$ obtained during 72 h (4320 min) adsorption of I$_2$ in cyclohexane.

Time	TpBD-Me$_2$	TpBD-(OMe)$_2$	
/ min	q_t^{N+CO}/g·mol^{-1}	q_t^{N+O}/g·mol^{-1}	q_t^{EO}/g·mol^{-1}
1	0.045	0.048	0.003
5	0.26	0.86	0.60
10	1.00	1.63	0.63
15	1.30	2.11	0.81
20	1.70	2.63	0.93
30	2.09	3.40	1.31
40	2.65	4.07	1.42
60	3.35	4.88	1.53
80	4.00	5.70	1.70
90	4.30	6.41	2.11
120	5.09	7.37	2.28
150	5.69	7.85	2.16
180	6.26	8.57	2.31
240	7.00	9.43	2.43
300	7.56	10.82	3.26
360	8.04	11.44	3.4
480	8.82	12.20	3.38
600	9.39	13.11	3.72
1440	11.43	15.27	3.84
1800	11.69	15.60	3.91
2880	12.34	16.32	3.98
3240	12.47	16.41	3.94
4320	12.78	16.66	3.88

Table S7 Summary of the values of q_e^{N+CO} (exp. q_e^{N+CO}) of TpBD-Me$_2$ and the values of q_e^{N+O} and q_e^{EO} (exp. q_e^{N+O}, q_e^{EO}) of TpBD-(OMe)$_2$ obtained by 72 h adsorption of I$_2$ in cyclohexane at initial concentration of 100.25 mg·L^{-1} and the calculated value of q_e^{N+CO}, q_e^{N+O} and q_e^{EO} (cal. q_e^{N+CO}, q_e^{N+O} and q_e^{EO}) from fitting of their adsorption kinetics profiles according to pseudo-first-order or pseudo-second-order models. The kinetic parameters obtained by fitting according to pseudo-first-order or pseudo-second-order models are also listed in the Table S7.

COFs	exp. q_e^{uc} /g·mol^{-1}	Pseudo-first-order model			Pseudo-second-order model		
		cal. q_e^{uc} /g·mol^{-1}	k_1/min^{-1}	R^2	cal. q_e^{uc} /g·mol^{-1}	k_2/mol· g^{-1}·min^{-1}	R^2
q_e^{N+CO}	12.78	11.76	0.004	0.969	12.96	4.004E-4	0.995
q_e^{N+O}	16.66	15.45	0.005	0.965	16.91	3.698 E-4	0.993
q_e^{EO}	3.88	3.75	0.007	0.931	4.03	0.003	0.967

Table S8 Summary of the q_e (mg·g^{-1}), q_e^{uc} (g·moL^{-1}) and q_e^{Mol} values of TpBD-Me$_2$ and TpBD-(OMe)$_2$ COFs obtained by 72 h adsorption of I$_2$ in cyclohexane at different initial I$_2$ concentrations ($C_{I_2}^0$, mg·L^{-1}).

$C_{I_2}^0$/ mg·L^{-1}	TpBD-Me$_2$			TpBD-(OMe)$_2$		
	q_e /mg·g^{-1}	q_e^{uc} /g·mol^{-1}	q_e^{Mol}	q_e /mg·g^{-1}	q_e^{uc} /g·mol^{-1}	q_e^{Mol}
100.25	80.77	76.66	0.302	95.61	99.93	0.394
201.13	134.95	128.09	0.505	170.94	178.66	0.704
500.5	277.72	263.60	1.039	333.77	348.84	1.374
821.34	389.22	369.43	1.456	451.86	472.26	1.861
998.02	433.79	411.73	1.622	518.95	542.38	2.137
1505.58	533.10	505.99	1.994	643.54	672.60	2.650

Table S9 Summary of the fitting results of I$_2$ adsorption isotherms in terms of q_e (mg·g^{-1}) of TpBD-Me$_2$ and TpBD-(OMe)$_2$ in cyclohexane obtained by Table S8 according to Langmuir and Freundlich models.

COFs	Langmuir model			Freundlich model		
	q_m /mg·g^{-1}	K_L /L·mg^{-1}	R^2	K_F /mg$^{1-1/n}$g^{-1}L$^{1/n}$	1/n /mg·L^{-1}	R^2
TpBD-Me$_2$	681.67	0.003	0.982	20.97	0.474	0.992
TpBD-(OMe)$_2$	728.77	0.006	0.921	45.98	0.390	0.998

Table S10 Summary of the fitting results of I$_2$ adsorption isotherms in terms of q_e^{uc} (g·mol^{-1}) of TpBD-Me$_2$ and TpBD-(OMe)$_2$ in cyclohexane obtained by Table S8 according to Langmuir and Freundlich models.

COFs	Langmuir model			Freundlich model		
	q_m^{uc} /g·mol^{-1}	K_L /L·mg^{-1}	R^2	K_F /gL$^{1/n}$	1/n /mg·L^{-1}	R^2
TpBD-Me$_2$	646.99	0.003	0.982	19.90	0.474	0.992
TpBD-(OMe)$_2$	761.68	0.006	0.921	48.06	0.390	0.998

Table S11 Summary of the element atomic concentration of TpBD-Me$_2$@I$_2$ and TpBD-(OMe)$_2$@I$_2$ after iodine adsorption derived from the results of survey XPS spectra in Figure S17.

COFs	C	O	N	I
TpBD-Me$_2$@I$_2$	69.26%	24.48%	5.7%	0.56%
TpBD-(OMe)$_2$ @I$_2$	65.36%	30.17%	3.65%	0.82%

Table S12 Summary of I$_2$ adsorption capacity of reported porous materials in organic solvent.

Types	Porous materials	adsorption capacity / mg·g^{-1}	Reference
MOFs	UiO-66-PYDC	1250	S1
	[Cu$_3$(μ$_2$-O)$_2$(p-tr$_2$Ph)$_2$ (HCOO)] [NO$_3$]·3DMF·3H$_2$O	1150	S2
	Th-BDAT	1046	S3
	[Eu$_2$(TATAB)$_2$]·xDMF·yH$_2$O	758.72	S4
	Lac-Zn	755	S5
	Th-TATAB	750	S6
	[Cu$_2$(TBDA-Cl) (H$_2$O)·10DMF·30H$_2$O]$_n$	548.2	S7
	Th-TTHA	528	S8
	[Co$_2$(H$_2$BATD)(DMF)$_2$]·2.5DMF·0.5H$_2$O	480.99	S9
	Th-SINAP-8	473	S10
	SCNU-Z5	442	S11
	UiO-66	401	S1
	NS-1	320.5	S12
	MIL-101-NH$_2$	311	S13
	Th-UiO-66-(NH$_2$)$_2$	300	S14
	SCNU-Z4	237	S15
	NUC-3	212.04	S16
	MOF-5	155	S17
	[Cd (nds) (bimh)$_2$ $\cdot$ (bimh)]n	148.5	S18
	U-TATAB	146.72	S19
	CuAceAd crystals	144	S20
	MIL-101(Cr)	69.8	S21
POPs	Azo-Car-CF$_3$	1198.00	S22
	DTC-OP2	915.19	S23

	TTDP-3	784	S24
	TTDP-2	694.8	S24
	TTDP-1	682.6	S24
	P-TzTz	568.28	S25
	DTC-OP3	528.45	S23
	TPAPyD-CMP	333.8	S26
	NiP-CMP	326	S27
	TPFM	293.3	S28
	NRPOP-1	285.7	S29
	POBI	239	S30
	NRPOP-2	212.8	S29
COFs	P-COFs	1295.20	S31
	PA-TT COF	750	S32
	TpBD-(OMe)₂	**728.77**	**This work**
	TpPa	727.64	S33
	TpBD-Me₂	**681.67**	**This work**
	TpPa-CuCl₂	674.48	S33
	DaTd-COF	666.79	S34
	Cu$_x$Pc-COFs	492.27	S35
	Hz-COF	173	S36
	Tfp-BD	99.9	S37
	TFB-BD	99.9	S38

Table S13 Summary of the values of Q_t, Q_t^{uc} of TpBD-Me₂ and TpBD-(OMe)₂ obtained during 72 h (4320 min) adsorption of I$_3^-$ in KI/I₂ aqueous solution.

Time /	TpBD-Me₂		TpBD-(OMe)₂	
min	Q_t/mg·g^{-1}	Q_t^{uc}/mg·g^{-1}	Q_t/mg·g^{-1}	Q_t^{uc}/mg·g^{-1}
1	0.82	0.78	5.1	5.33
5	6.88	6.53	13.42	14.03
10	13.14	12.47	20.16	21.07
20	17.50	16.61	24.12	25.21
30	24.32	23.08	28.76	30.06
40	27.04	25.67	34.48	36.04
60	34.68	32.92	40.40	42.22
80	41.16	39.07	45.52	47.58

90	45.86	43.53	50.42	52.70
120	50.62	48.05	55.46	57.96
150	55.94	53.10	60.98	63.73
180	60.50	57.42	65.42	68.37
240	69.10	65.59	72.70	75.98
300	73.38	69.65	79.52	83.11
360	80.40	76.31	85.32	89.17
480	88.58	84.08	92.66	96.84
600	93.82	89.05	100.10	104.62
1440	111.62	105.94	117.18	122.47
1800	115.9	110.01	120.48	125.92
2880	121.78	115.59	124.08	129.68
3240	122.78	116.54	124.7	130.33
4320	123.68	117.39	125.18	130.83

Table S14 Summary of the experimental values of Q_e (exp. Q_e) of TpBD-Me$_2$ and TpBD-(OMe)$_2$ obtained by 72 h adsorption of I$_3^-$ in KI/I$_2$ aqueous solution at initial concentration of 66.73 mg·L^{-1} of I$_2$ and the calculated value of Q_e (cal. Q_e) from fitting of their adsorption kinetics profiles according to pseudo-first-order or pseudo-second-order models. The kinetic parameters obtained by fitting according to pseudo-first-order or pseudo-second-order models are also listed in the Table S14.

COFs	exp. Q_e /mg·g^{-1}	Pseudo-first-order model			Pseudo-second-order model		
		cal. Q_e /mg·g^{-1}	k_1/min^{-1}	R^2	cal. Q_e /mg·g^{-1}	k_2/min^{-1}	R^2
TpBD-Me$_2$	123.68	115.21	0.004	0.961	126.48	4.343E-5	0.992
TpBD-(OMe)$_2$	125.18	117.01	0.005	0.938	127.36	5.249E-5	0.979

Table S15 Summary of the experimental values of Q_e^{uc} (exp. Q_e^{uc}) of TpBD-Me$_2$ and TpBD-(OMe)$_2$ obtained by 72 h adsorption of I$_3^-$ in KI/I$_2$ aqueous solution at initial concentration of 66.73 mg·L^{-1} of I$_2$ and the calculated value of Q_e^{uc} (cal. Q_e^{uc}) from fitting of their adsorption kinetics profiles according to pseudo-first-order or pseudo-second-order models. The kinetic parameters obtained by fitting according to pseudo-first-order or pseudo-second-order models are also listed in the Table S15.

COFs	exp. Q_e^{uc} /g·mol^{-1}	Pseudo-first-order model			Pseudo-second-order model		
		cal. Q_e /g·mol^{-1}	k_1/min^{-1}	R^2	cal. Q_e /mg·g^{-1}	k_2/ mol· g^{-1}·min^{-1}	R^2
TpBD-Me$_2$	117.39	109.35	0.004	0.961	120.05	4.576E-5	0.991
TpBD-(OMe)$_2$	130.83	122.30	0.005	0.938	133.10	5.023E-5	0.979

Table S16 Summary of the Q_e (mg·g^{-1}) and Q_e^{uc} (g·moL^{-1}) values of TpBD-Me$_2$ and TpBD-(OMe)$_2$ obtained by 72 h adsorption of I$_3^-$ in in KI/I$_2$ aqueous solution at different initial I$_2$ concentrations ($C_{I_2}^0$, mg·L^{-1}).

$C_{I_2}^0$	TpBD-Me$_2$		TpBD-(OMe)$_2$	
	Q_e/mg·g^{-1}	Q_e^{uc}/g·moL^{-1}	Q_e/mg·g^{-1}	Q_e^{uc}/g·moL^{-1}
66.73	123.68	117.39	125.18	130.83
142.52	216.94	205.91	225.80	235.99
214.82	300.18	284.92	322.48	337.04
396.51	468.24	444.43	515.96	539.26
700.72	703.24	667.48	759.80	794.10

Table S17 Summary of the fitting results of I$_2$ adsorption isotherms in terms of Q_e (mg·g^{-1}) of TpBD-Me$_2$ and TpBD-(OMe)$_2$ COFs in KI/I$_2$ aqueous solution obtained by Table S16 according to Langmuir and Freundlich models.

COFs	Langmuir model			Freundlich model		
	Q_m /mg·g^{-1}	K_L /L·mg^{-1}	R^2	K_F /mg$^{1-1/n}$g^{-1}L$^{1/n}$	1/n /mg·L^{-1}	R^2
TpBD-Me$_2$	939.56	0.007	0.925	41.44	0.481	0.990
TpBD-(OMe)$_2$	997.13	0.009	0.948	49.77	0.472	0.993

Table S18 Summary of the fitting results of I$_2$ adsorption isotherms in terms of Q_e^{uc} (g·mol^{-1}) of TpBD-Me$_2$ and TpBD-(OMe)$_2$ COFs in KI/I$_2$ aqueous solution obtained by Table S16 according to Langmuir and Freundlich models.

COFs	Langmuir model			Freundlich model		
	Q_m^{uc} /g·mol^{-1}	K_L /L·mg^{-1}	R^2	K_F /gL$^{1/n}$	1/n /mg·L^{-1}	R^2
TpBD-Me$_2$	891.77	0.007	0.925	39.34	0.481	0.990
TpBD-(OMe)$_2$	1042.15	0.009	0.948	52.02	0.472	0.993

Table S19 Summary of the element atomic concentration of TpBD-Me$_2$@I$_3^-$ and TpBD-(OMe)$_2$ @I$_3^-$ after I$_3^-$ adsorption derived from the results of survey XPS spectra in Figure S21.

COFs	C	O	N	I
TpBD-Me$_2$@I$_3^-$	79.8%	11.02%	8.13%	1.05%
TpBD-(OMe)$_2$ @I$_3^-$	80.79%	11.93%	5.76%	1.52%

References

[S1] Wang, Z.; Huang, Y.; Yang, J.; Li, Y.; Zhuang, Q.; Gu, J. The Water-Based Synthesis of Chemically Stable Zr-Based MOFsUsing Pyridine-Containing Ligands and Their Exceptionally High Adsorption Capacity for Iodine. *Dalton Trans.* **2017**, 46, 7412-7420.

[S2] Xu, T.; Li, J.; Jia, M.; Li, G.; Liu, Y. Contiguous Layer Based Metal–Organic Framework with Conjugated π-Electron Ligand for High Iodine Capture. *Dalton Trans.* **2021**, 50, 13096-13102.

[S3] Ju, Y.; Li, Z.; Qiu, J.; Li, X.; Yang, J.; Zhang, Z.; He, M.; Wang, J.; Lin, J. Adsorption and Detection of Iodine Species by a Thorium-Based Metal−Organic Framework. *Inorg. Chem.* **2023**, 62, 8158-8165.

[S4] Zhao, Y.; Zhang, N.; Wang, Y.; Bai, F.; Xing, Y.; Sun, L. Ln-MOFs with Window-Shaped Channels Based on Triazine Tricarboxylic Acid as a Linker for the Highly Efficient Capture of Cationic Dyes and Iodine. *Inorg. Chem. Front.* **2021**, 8, 1736-1746.

[S5] Xu, L.; Zheng, Q.; Wang, Y.; Jiang, L.; Jiang, J.; Qiu, J. A Pillared Double-Wall Metal-Organic Framework Adsorption Membrane for the Efficient Removal of Iodine from Solution *Sep. Purif. Technol.* **2021**, 274, 118436.

[S6] Zhang, N.; Sun, L.; Xing, Y.; Bai, F. A Double-Walled Thorium-Based Metal−Organic Framework as a Promising Dual-Function Absorbent for Efficiently Capturing Iodine and Dyes *Cryst. Growth Des.* **2019**, 19, 5686-5695.

[S7] Cai, H.; Zeng, G.; You, Z.; Wang, C.; Sun, L.; Bai, F.; Xing, Y. Cu(II) and Zn(II) Frameworks Constructed by Directional Tuning of Diverse Substituted Groups on a Triazine Skeleton and Supermassive Adsorption Behavior for Iodine and Dyes. *Dalton Trans.* **2022**, 51, 5457-5470.

[S8] Zhang, N.; Sun, L.; Bai, F.; Xing, Y. Thorium-Organic Framework Constructed with a Semirigid Triazine Hexacarboxylic Acid Ligand: Unique Structure with Thorium Oxide Wheel Clusters and Iodine Adsorption Behavior. *Inorg. Chem.* 2020, 59, 3964-3973.

[S9] Liu, M.; Cai, H.; Jiang, S.; Xing, Y.; Bai, F. Construction of a Triazine Polycarboxylate Co-MOF with Flexible and Rigid Coordination Arms as well as Excellent Catalytic Reduction and Adsorption Properties. *Dalton Trans.* **2023**, 52, 6773-6781.

[S10] Li, Z.; Yue, Z.; Ju, Y.; Wu, X.; Ren, Y.; Wang, S.; Li, Y.; Zhang, Z.; Guo, X.; Lin, J.

Ultrastable Thorium Metal−Organic Frameworks for Efficient Iodine Adsorption *Inorg. Chem.* **2020**, 59, 4435-4442.

[S11] Huang, J.; Hu, H.; Deng, S.; Cai, S.; Fan, J.; Zhang, W.; Zheng, S. A Ni(II) metal–organic framework with helical channels for the capture of iodine via guest exchange induced amorphization. *New J Chem.* **2022**, 46, 7144-7152.

[S12] Hu, H.; Chen, F.; Zhang, Z.; Liu, D.; Liang, Y.; Chen, Z. Heterometallic Metal-Organic Framework Based on [Cu$_4$I$_4$] and [Hf$_6$O$_8$] Clusters for Adsorption of Iodine. *Front. Chem.* **2022**, 10, 864131.

[S13] Falaise, C.; Volkringer, C.; Facqueur, J.; Bousquet, T.; Gasnot, L.; Loiseau, T. Capture of Iodine in Highly Stable Metal–Organic Frameworks: a Systematic Study. *Chem. Commun.* **2013**, 49, 10320-10322.

[S14] Li, Z.; Ju, Y.; Lu, H.; Wu, X.; Yu, X.; Li, Y.; Wu, X.; Zhang, Z.; Lin, J.; Qian, Y. Boosting the Iodine Adsorption and Radioresistance of Th-UiO-66 MOFs via Aromatic Substitution. *Chem. Eur. J.* **2020**, 27, 1286-1291.

[S15] Wang, G.; Huang, J.; Huang, X.; Deng, S.; Zheng, S.; Cai, S.; Fan, J.; Zhang, W. A Hydrolytically Stable Cage-Based Metal–Organic Framework Containing two Types of Building Blocks for the Adsorption of Iodine and Dyes. *Inorg. Chem. Front.* **2021**, 8, 1083-1092.

[S16] Chen, H.; Fan, L.; Zhang, X.; Ma, L. Robust Heterometallic Tb^{III}/Mn^{II}–Organic Framework for CO$_2$/CH$_4$ Separation and I$_2$ Adsorption. *ACS Appl. Nano Mater.* **2020**, 3, 2680-2686.

[S17] Yu, R.; Li, Q.; Zhang, T.; Li, Z.; Xia, L. Zn, O Co-Adsorption Based on MOF-5 for Efficient Capture of Radioactive Iodine. *Process Saf. Environ.* **2023**, 174, 770-777.

[S18] Yang, Y.; Tu, C.; Shi, J.; Zhao, T.; Liu, Z.; Cheng, F.; Luo, F. Highly Stable Cd(II)-MOFs Based on 2,6-Naphthanlenedisulfonate and Bisimidazole Ligands: A New Platform for Selective Detection of Cu^{2+} and Efficient Removal of Iodine. *J. Solid State Chem.* **2021**, 302, 122439.

[S19] Zhang, N.; Xing, Y.; Bai, F. A Uranyl-Organic Framework Featuring Two-Dimensional Graphene-like Layered Topology for Efficient Iodine and Dyes Capture. *Inorg. Chem.* **2019**, 58, 6866-6876.

[S20] Li, M.; Yuan, G.; Zeng, Y.; Yang, Y.; Liao, J.; Yang, J.; Liu, N. Flexible surface‑supported MOF membrane via a convenient approach for efficient iodine adsorption. *J. Radioanal. Nucl. Ch.* **2020**, 324, 1167-1177.

[S21] Al Lafi, A. G.; Assfour, B.; Assaad, T. Metal Organic Framework MIL‑101(Cr): Spectroscopic Investigations to Reveal Iodine Capture Mechanism. *J. Inorg. Organomet. P.* 2020, 30, 1218-1230.

[S22] Li, L.; Sun, Z.; Yang, A.; Zhang, X.; Zhu, X.; Li, W.; Liu, Y.; Luan, J. A Novel Azo-Linked Polymer Bearing Trifluoromethyl Groups for I$_2$ Capture. *Macromol. Rapid Comm.* **2023**, 44, 2200982.

[S23] Thurakkal, L.; Cheekatla, S.; Porel, M. Superfast Capture of Iodine from Air, Water, and Organic Solvent by Potential Dithiocarbamate-Based Organic Polymer. *Int. J. Mol. Sci.* **2023**, 24, 1466.

[S24] Du, W.; Qin, Y.; Ni, C.; Dai, W.; Zou, J. Efficient Capture of Volatile Iodine by Thiophene-Containing Porous Organic Polymers. *ACS Appl. Polym. Mater.* **2020**, 2, 5121-5128.

[S25] Pan, X.; Ding, C.; Zhang, Z.; Ke, H.; Cheng, G. Functional Porous Organic Polymer with High S and N for Reversible Iodine Capture. *Micropor. Mesopor. Mat.* **2020**, 300, 110161.

[S26] Yang, X.; Duan, L.; Ran, X.; Ran, B.; Yi, S. Two Nitrogen‑Rich Conjugated Microporous Polymers for Efficient Iodine Sequestration and Removal. *J. Polym. Res.* **2022**, 29, 499.

[S27] Sigen, A.; Zhang, Y.; Li, Z.; Xia, H.; Xue, M.; Liu, X.; Mu, Y. Highly Efficient and Reversible Iodine Capture Using a Metalloporphyrin-Based Conjugated Microporous Polymer. *Chem. Commun.* **2014**, 50, 8495-8498.

[S28] Liu, L.; Song, C.; Kong, A. Nitrogen and Sulfur-Enriched Porous Bithiophene-Melamine Covalent Organic Polymers for Effective Capture of CO_2 and Iodine. *Mater. Lett.* **2020**, 277, 128291.

[S29] Mohan, A.; Al-Sayah, M. H.; Ahmed, A.; El-Kadri, O. M. Triazine‑Based Porous Organic Polymers for Reversible Capture of Iodine and Utilization in Antibacterial Application. *Sci. Rep.* **2022**, 12, 2638.

[S30] Yang, M.; Shi, W.; Liu, S.; Xu, K. Multifunctional Diphenyl Ether-Based, Cross-Linked Polyisocyanide for Efficient Iodine Capture and NO_2^-/SO_3^{2-} Electrochemical Probing. *Colloid. Surface. A* **2022**, 642, 128680.

[S31] Li, Y.; Li, X.; Li, J.; Liu, W.; Cheng, G.; Ke, H. Phosphine-Based Covalent Organic Framework for Highly Efficient Iodine Capture. *Micropor. Mesopor. Mat.* **2021**, 325, 111351.

[S32] Yan, X.; Yang, Y.; Li, G.; Zhang, J.; He, Y.; Wang, R.; Lin, Z.; Cai, Z. Thiophene-Based Covalent Organic Frameworks for Highly Efficient Iodine Capture. *Chinese Chem. Lett.* **2023**, 34, 107201.

[S33] Jing, L.; Cheng, C.; Wang, B.; Wang, S.; Xie, R.; Xia, H.; Wang, D. Controlled Iodine Phase Transfer of Covalent Organic Framework Membranes for Instant but Sustained Disinfection. *Langmuir* **2023**, 39, 597-609.

[S34] Wu, Z.; Wei, W.; Ma, J.; Luo, J.; Zhou, Y.; Zhou, Z.; Liu, S. Adsorption of Iodine on Adamantane-Based Covalent Organic Frameworks. *Chem. Select* **2021**, 6, 10141-10148.

[S35] Liu, X.; Zhang, A.; Ma, R.; Wu, B.; Wen, T.; Ai, Y.; Sun, M.; Jin, J.; Wang, S.; Wang, X. Experimental and Theoretical Insights into Copper Phthalocyanine-Based Covalent Organic Frameworks for Highly Efficient Radioactive Iodine Capture. *Chinese Chem. Lett.* **2022**, 33, 3549-3555.

[36] Mokhtari, N.; Dinari, M. Developing Novel Amine-Linked Covalent Organic Frameworks towards Reversible Iodine Capture. *Sep. Purif. Technol.* **2022**, 301, 121948.

[S37] Song, S.; Shi, Y.; Liu, N.; Liu, F. C=N Linked Covalent Organic Framework for the Efficient Adsorption of Iodine in Vapor and Solution. *RSC Adv.* **2021**, 11, 10512-10523.

[S38] Song, S.; Shi, Y.; Liu, N.; Liu, F. Theoretical Screening and Experimental Synthesis of Ultrahigh-Iodine Capture Covalent Organic Frameworks. *ACS Appl. Mater. Interfaces* **2021**, 13, 10513-10523.